Influence of Prior Warm Deformation on Cementite Spheroidization Process in a Low-Alloy Medium Carbon Steel

J. ARRUABARRENA, B. LÓPEZ, and JOSE M. RODRIGUEZ-IBABE

Warm deformations have been applied to a low-alloy medium carbon steel (AISI 5140) to promote faster spheroidization during soft annealing treatments. The application of warm deformation leads to the fragmentation of cementite lamellae and the formation of defects on both cementite and the matrix. This induces faster lamellae break-up according to a boundary splitting mechanism, which is responsible for the improved spheroidization after annealing. The substructure developed in the matrix enhances pipe diffusion through the sub-boundaries, which helps the lamellae terminations to coarsen and causes lamellae fast splitting and finally yields a coarse cementite particle distribution. When deforming up to $\varepsilon = 0.3$, almost fully spheroidized microstructures are obtained after annealing at 993 K (720 °C), independently of the initial pearlite features. By means of the EBSD technique, it has been observed that the applied warm deformation, in addition to enhancing the degree of spheroidization, allows a much finer microstructure to be formed after annealing. Grain refinement takes place as a consequence of a continuous recrystallization process, which is directly related to cementite spheroidization in the long term.

DOI: 10.1007/s11661-013-2066-3

I. INTRODUCTION

IT is well known that the lamellar morphology of the pearlite formed after conventional bar rolling of medium carbon steels limits up to certain point its cold formability.[1,2] In the industrial procedure, low cooling rates are usually imposed just after rolling, in order to provide a coarse pearlite microstructure which is desirable from the point of view of softness and ductility. When high deformation processes are required, such as cold headability or extrusion, the as-rolled condition is not appropriate enough and soft annealing treatments need to be applied. During these treatments, the ferrite matrix softens and the lamellar cementite evolves into a globularized morphology with improved ductility. As annealing treatments can be both time and energy consuming, different new processes have been proposed to reduce treatment duration, some of them related to the conditioning of the initial microstructure prior to annealing treatment and others modifying the process by applying severe deformation or by changing the treating cycle.[3–7]

The initial pearlite features become a critical aspect in order to reduce annealing production costs.[8–10] The initial microstructure conditioning, either by modifying the cooling rates applied after rolling or even by changing the rolling schedule, may lead to significant reduction of the treatment time and consequently to a reduction in the manufacturing costs.[2,3] Some research done on pearlite deformation-assisted technologies, such as severe plastic deformation (SPD) and heavy warm deformation (HWD) techniques, has shown that high deformation applications lead to an ultrafine grained microstructure development, in addition to significantly enhancing pearlite spheroidization rates.[11–16]

It is necessary to take into account that in conventional soft annealing the morphological changes on the cementite are mainly generated through the migration of defects present in the cementite lamella and through the break-up related to the Rayleigh instability phenomena.[17–20] Crystalline defects such as lamella terminations and holes provide high curvature areas. According to the Gibbs-Thompson effect, the solute concentration in the vicinity of these places is higher than in the matrix adjacent to the flat areas of the lamella. This difference establishes a constant solute flux away from the tips constituted by such defects, so the defect migrates while the nearby flat areas, either in the same lamella or in the neighboring lamella, coarsen. The continuous solute transference may give rise to the formation of a ridge along both the edge of the lamella and the cementite edges surrounding a hole. As the ridge grows the structure along its length becomes unstable against a Rayleigh perturbation of sufficient wavelength. The growth in amplitude of such a perturbation is enhanced by the continuation of the edge coarsening, up to a point where the cylinder-like shape breaks into spheroids.

For warm deformed microstructures it is reported that in addition to defect migration and break-up, cementite sub-boundary splitting also contributes to cementite spheroidization.[18,21,22] Boundary splitting is the consequence of the presence of sub-boundaries within the cementite. These sub-boundaries are assumed

J. ARRUABARRENA, Ph.D. Student, and B. LÓPEZ and JOSE M. RODRIGUEZ-IBABE, Professors, are with the CEIT and Tecnun, University of Navarra, P° de Manuel Lardizabal 15, 20018 San Sebastian, Basque Country, Spain. Contact e-mail: jmribabe@ceit.es

Manuscript submitted June 13, 2013.
Article published online October 19, 2013

to be introduced into a lamella by deformation and posterior restoration or by phase transformation processes. At triple points between cementite sub-grains and the ferrite matrix, the establishment of the local equilibrium of the surface tensions involves the formation of a groove along the sub-boundary. The chemical potential gradient due to the curvature at the interface promotes mass transport away from the groove while at the same time involving continuous elimination of the sub-boundary, and final lamella splitting.

Unfortunately, despite their potential benefits, the required deformation levels at subcritical temperatures (usually applied strains $\varepsilon > 1$[11–15]) are difficult to attain in current conventional bar rolling mills, and as a result their use remains limited. Instead, the application of prior slight warm deformations, in the range $\varepsilon < 0.5$, could be possible in new, more powerful industrial installations, which would allow the required annealing time for a certain degree of spheroidization to be reduced. This study analyzes the influence of the initial microstructure (fine and coarse pearlite), in combination with different deformation levels applied at the end of transformation, on spheroidization in a low-alloy medium carbon steel.

II. EXPERIMENTAL PROCEDURE

The steel studied is a low-alloy medium carbon steel containing 0.40 pct C, 0.78 pct Mn, 1.0 pct Cr, 0.17 pct Si, and 0.027 pct S in wt pct (data supplied by the steel manufacturer). Heat treatments and compression tests were conducted on dilatometry cylindrical samples 8 mm in length and 4 mm in diameter and machined from a 25-mm-diameter hot-rolled bar using a Bähr DIL805A/D quenching and deformation dilatometer (Bähr-Thermoanalyse GmbH, Hullhorst, Germany).

The specimens were austenitized at 1123 K (850 °C) for 15 minutes, cooled down at a rate of 20 K/s to 973 K or 903 K (700 °C or 630 °C), and maintained at these temperatures for 12 and 7 minutes, respectively, as shown in the scheme of Figure 1. The temperature was monitored by a thermocouple fixed on each sample, and the cooling was conducted by pumping He into the chamber. The holding times were selected to assure a nearly complete transformation of the austenite and to avoid at the same time possible initial spheroidization phenomena related to longer holding times. Assuming equivalence between the transformed fraction and sample dilatation, dilatometry trials showed that these times provided about a 90 pct austenite transformation at each temperature. The remaining austenite would transform during the cooling stage at 1 K/s up to room temperature. Phase transformation at 973 K (700 °C) provided the formation of a coarse pearlite, whereas at 903 K (630 °C) a fine pearlite was obtained.

In order to evaluate the influence of strain application on subsequent annealing treatments, warm deformation was imposed applying $\varepsilon = 0.1$, 0.3, and 0.5 compressive strains at a 1 s^{-1} strain rate at the end of the isothermal holding, followed by cooling down to room temperature at 1 K/s. The spheroidization thermal cycles were carried out considering both non-deformed and deformed conditions. The specimens were annealed sub-critically for 2 hours (short cycle) or 10 hours (long cycle), respectively (Figure 1). Preliminary dilatometry tests showed that the critical temperature A_{c1} of the steel is around 1043 K (770 °C). Considering this and also taking into account that in the presence of segregations austenitization may take place at temperatures lower than expected, an annealing temperature of 993 K (720 °C) was selected. The samples were introduced once the temperature in the furnace was stabilized at 993 K (720 °C), and they were taken out and air-cooled at room temperature after the specified holding times. The error in the treatment temperature is around ±1 K.

Metallographic observations were conducted by means of a field emission gun scanning electron microscopy (FEG-SEM, JEOL* JSM-700F) analysis prior to and after annealing treatments. Samples were sectioned along their longitudinal axis, selecting the region representative of the nominal strain according to the procedure described in Reference 23. The specimens were polished down to 1 μm and the microstructures were revealed by etching in 2 wt pct Nital.

The degree of spheroidization was quantified by image analysis over randomly selected FEG-SEM micrographs (at 10000 times magnification). The image analysis software provides accurate dimensional data for each cementite detected. Around 10^4 cementite particles were measured in each condition studied. Particles with an area smaller than 0.001 μm^2 were not considered in the analysis. According to the criteria used by O'Brien and Hosford,[1] cementite particles with an aspect ratio lower than 3 were considered to be spheroidized. Aspect ratio is defined as the relation between the length and the width of the cementite, and it is provided by the image analysis software. Thus, the overall degree of spheroidization was determined as the ratio between the area constituted by the spheroidized cementites and the total cementite area (spheroidized and non-spheroidized), normalized to area percentage. Cementite particle density was calculated as the number of cementites per unit area analyzed.

Crystallographic analysis was performed by using the Electron Backscatter Diffraction (EBSD) technique on samples polished with colloidal silica. In each scan an area of 200 × 200 μm^2 was analyzed using a 0.5-μm-long step size, except for the detailed scans in which 60 × 60 μm^2 areas and a 0.1-μm step size were used. Orientation imaging was carried out on a PHILIPS XL30cp** scanning electron microscope with W-filament, using TSL (TexSEM Laboratories, Provo, UT) equipment. Higher resolution orientation imaging analyses were conducted on the JEOL JSM-700F FEGSEM using

*JEOL is a trademark of Japan Electron Optics Ltd.

**PHILIPS is a trademark of FEI Company, Hillsboro, OR.

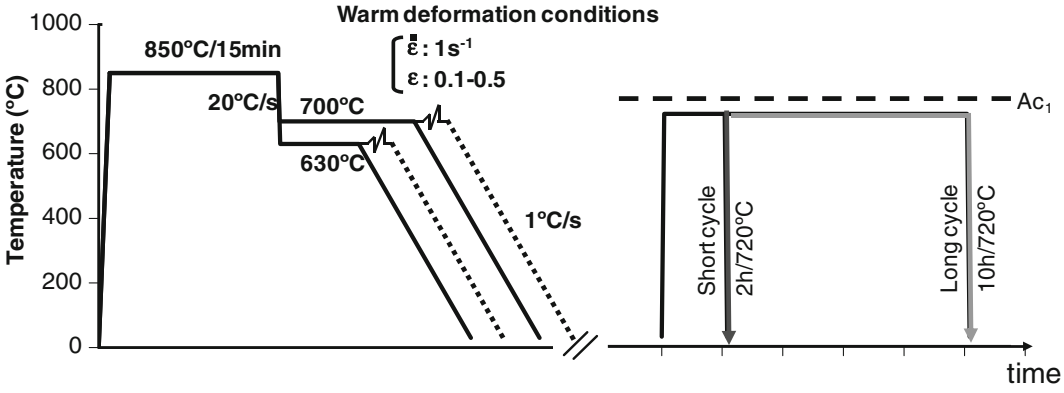

Fig. 1—Scheme of applied thermomechanical cycles.

Table I. Isothermally Transformed Pearlite Microstructural Parameters

Pearlite	Isothermal Treatment [K (°C)]	Proeutectoid Ferrite (pct)	Interlamellar Spacing (μm)	Lamella Thickness (μm)
Coarse	973 (700)	25.8 ± 2.9	0.274 ± 0.039	0.110 ± 0.003
Fine	903 (630)	7.2 ± 0.6	0.100 ± 0.020	0.050 ± 0.002

HKL Channel5 EBSD. Ferrite grain sizes were measured using 15 deg misorientation criteria.

Microhardness measurements were performed using a Vickers indenter with an applied load of 1 kg. The resulting indentation mark covered either pearlite or proeutectoid phases, so the determined value could well be considered as a local microstructure hardness value. A minimum of eight measurements were made at each condition and the mean value was determined.

III. RESULTS AND DISCUSSION

A. *Influence of the Applied Strain on Cementite Spheroidization*

The main microstructural features corresponding to the coarse and fine pearlite microstructures after the isothermal transformation are listed in Table I. The FEG-SEM micrographs of both pearlites are shown in Figure 2. The application of warm deformation at the end of isothermal transformation leads to several changes in the cementite lamellae and the ferrite matrix. Figure 3 is an example of the microstructure obtained after warm deforming the initial coarse pearlite ($\varepsilon = 0.3$). The deformation produces significant mechanical lamellae break-up, especially in those colonies where the cementite plates are aligned with the applied strain direction. A slight alignment of the pearlite lamellae perpendicular to the applied strain direction is also induced. As a consequence, the cementite plates present in the pearlite colonies lose their straight laminar morphology and become kinked and partially or completely fragmented. Deformation bands are also easily identified (Figures 3(a) and (b)).

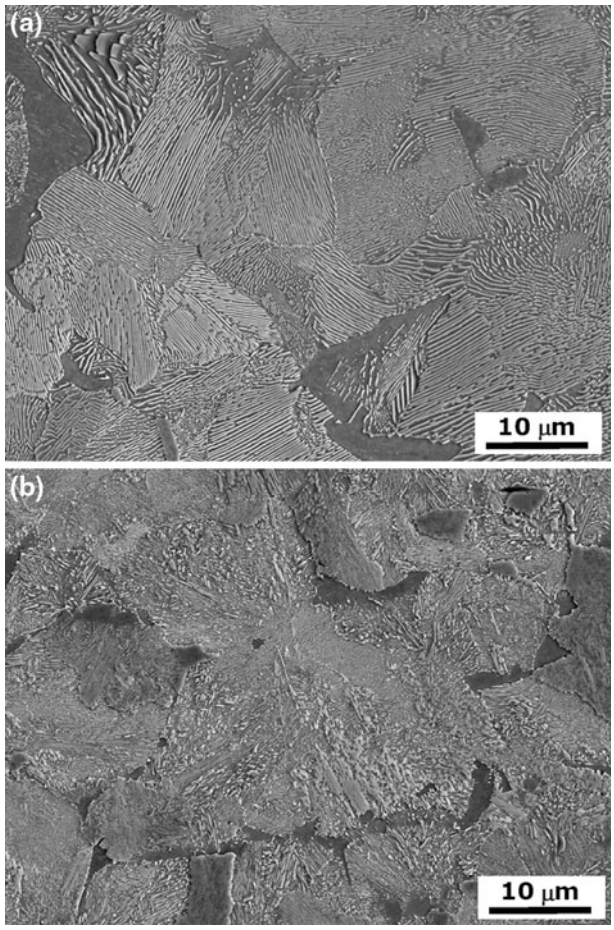

Fig. 2—(*a*) Coarse pearlite microstructure obtained after isothermal holding at 973 K (700 °C) for 12 min, and (*b*) fine pearlite microstructure obtained after 7 min at 903 K (630 °C).

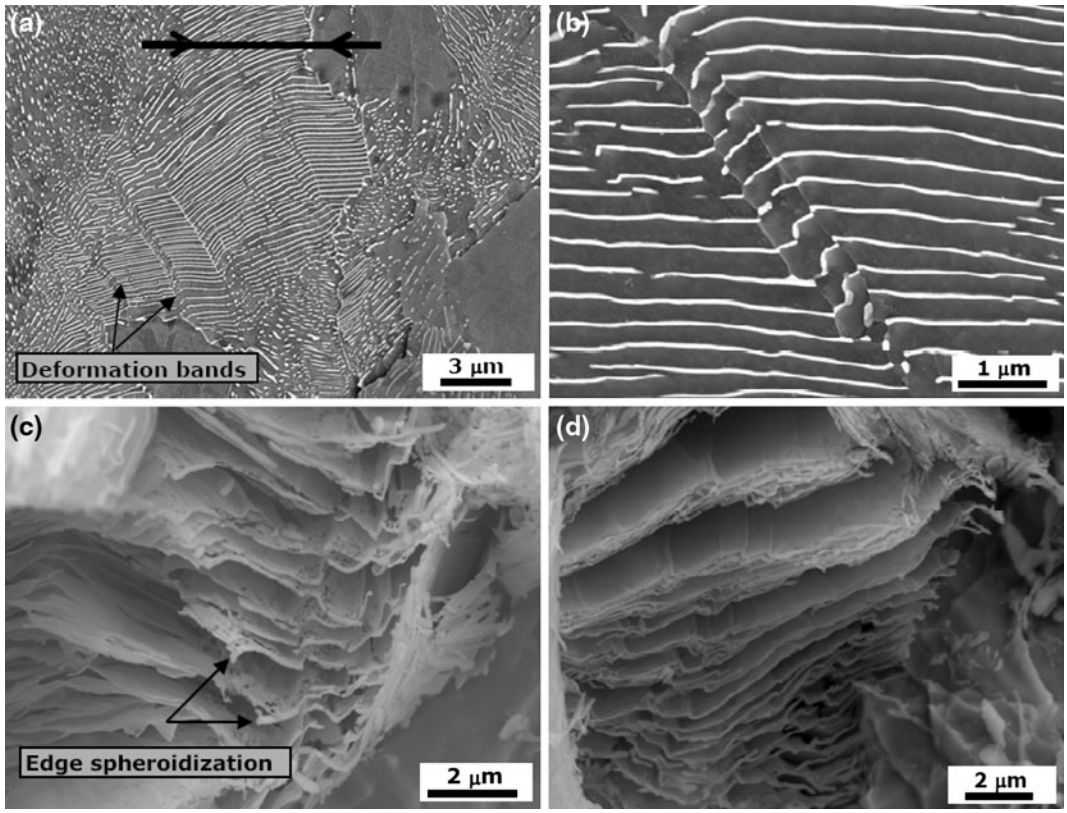

Fig. 3—(*a*) Crystallographic defects on the matrix, (*b*) detail of a deformation band, and (*c*, *d*) cementite features observed after deep etching on warm deformed [$T = 973$ K (700 °C), $\varepsilon = 0.3$] and non-deformed coarse pearlite, respectively. Arrows indicate direction of strain application.

Keeping the samples immersed in nital for 1 hour (deep nital etching), because the ferrite is preferentially etched, allows the 3D observation of the cementite lamellae. This technique reveals that after deformation the cementite lamellae exhibit a high number of imperfections, such as holes and kinks (compare Figures 3(c) and (d)). The initiation of the edge spheroidization process may be also observed (Figure 3(c)).

The microstructure evolution after deformation at different levels for a long spheroidization cycle is shown in Figure 4 for both coarse and fine pearlite conditions. The spheroidization is not completely homogeneous and certain pearlite colonies exhibit higher spheroidization than others, especially in non-deformed samples. This effect may arise from the presence of colonies where the cementites appear highly kinked, which makes the cementites more prone to spheroidization at annealing temperatures as kinks provide high curvature areas for the initiation of the mass transport processes governing spheroidization. In addition to the initial kinked constitution of the cementites, in warm deformed samples the microstructural heterogeneities may well be related to the colony alignment with respect to the applied strain. Some cementite lamellae may be affected differently when deforming, and as a consequence develop more or fewer defects or high curvature zones.

In the case of non-deformed microstructures, it is observed that several pearlite colonies maintain, at least in part, some of their initial geometrical features, despite the cementite lamellae being partially fragmented (Figures 4(a) and (b)) that is, the lamellar cementites break into shorter units but these units do not acquire spheroidized morphologies (globular shapes with an aspect ratio less than 3). In warm deformed microstructures, however, such differences are reduced and more homogeneous microstructures are obtained after annealing. The pearlite appears to be highly decomposed, especially when the applied deformation is $\varepsilon \geq 0.3$ (Figures 4(e) through (h)). In all the tested conditions, it is possible to observe a higher degree of spheroidization in the cementites located at prior austenite grain and pearlite colony boundaries. Finally, differences in the ferritic matrix are also observed, with well-defined recrystallized regions for higher deformation conditions (Figures 4(g) and (h), for example).

Cementite platelet break-up may be considered to occur according to two different mechanisms. One would be the fragmentation related to the strain imposed during warm deformation, which gives rise to lamellae mechanical break-up, as shown in Figure 3(a). The other would be the additional break-up due to spheroidization during the annealing treatment. The contribution of both effects to the overall cementite fragmentation depends either on the applied strain conditions or the annealing treatment parameters, respectively. During heat treatment, cementite lamellae split into globular units that coarsen as driven by the Ostwald ripening process. The microstructure evolution strongly depends on the applied deformation, such that as long as the deformation increases the resulting

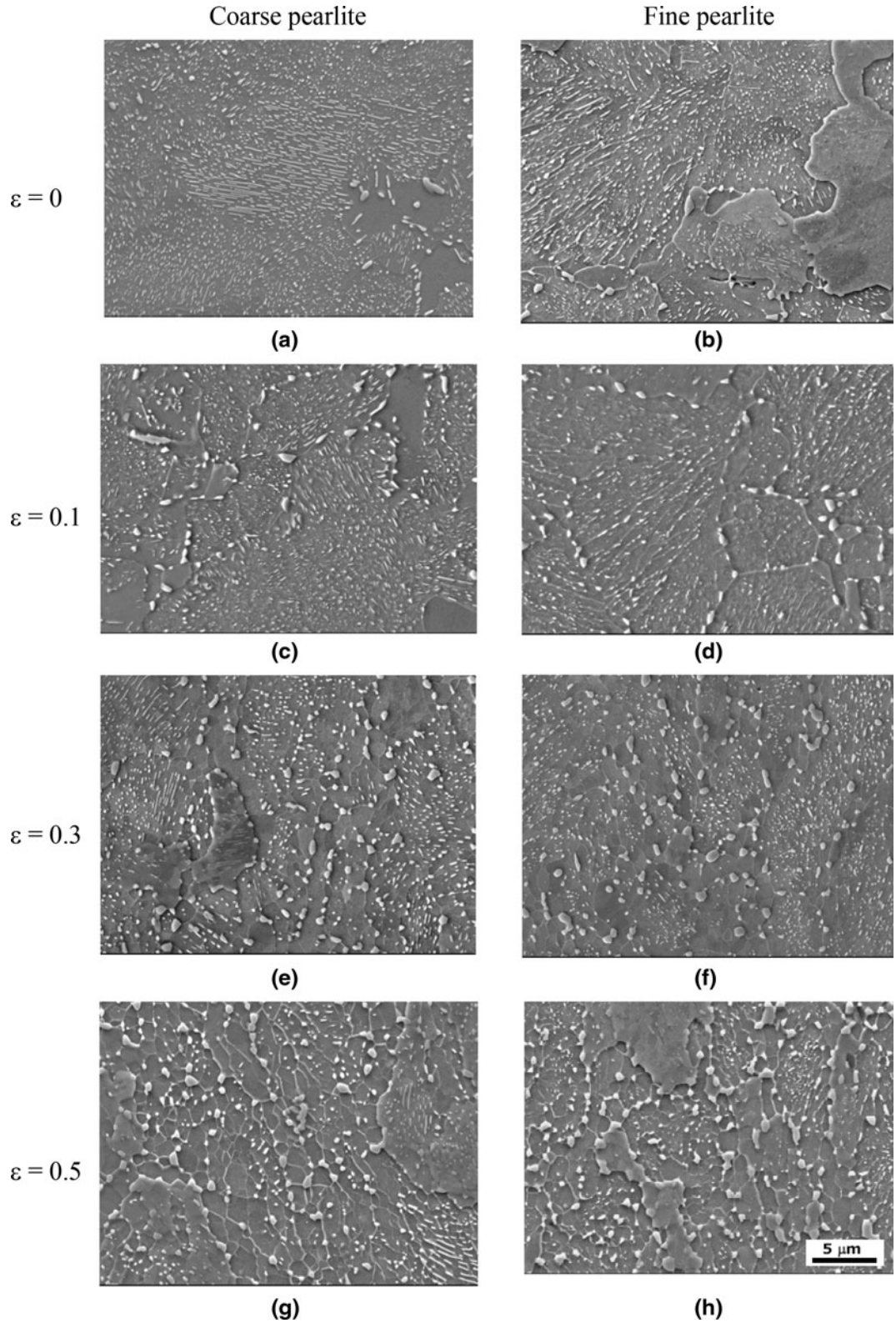

Fig. 4—Microstructures developed after the application of a long spheroidization cycle [10 h/993 K (720 °C)] on (*a*, *b*) $\varepsilon = 0$, (*c*, *d*) $\varepsilon = 0.1$, (*g*, *h*) $\varepsilon = 0.3$, and (*e*, *f*) $\varepsilon = 0.5$ warm deformed coarse and fine pearlite initial microstructures.

microstructure exhibits a higher degree of spheroidization after annealing, as can be observed when comparing Figures 4(c) and (d) with (g) and (h).

With regard to cementite growth, it is a widely known fact that, even in the non-deformed microstructure, cementites located at grain boundaries undergo higher

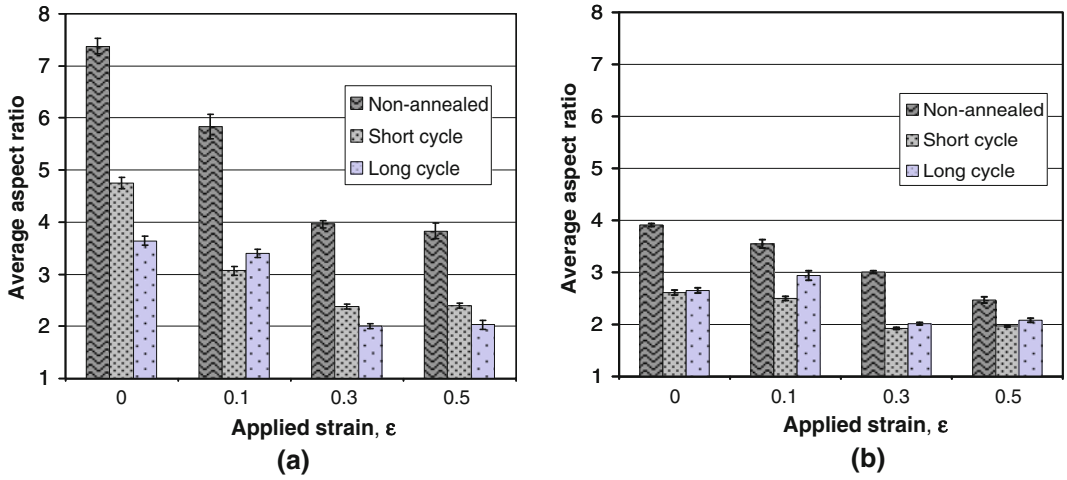

Fig. 5—Average cementite aspect ratio evolution as a function of the applied strain in (*a*) coarse pearlite and (*b*) fine pearlite after a short [2 h/993 K (720 °C)] and long annealing cycle [10 h/993 K (720 °C)].

coarsening.[24] Several examples can be observed in Figure 4, thus confirming the relevant role of enhanced pipe diffusion along boundaries in deformed microstructures. In addition, as recrystallization has taken place during annealing (mainly for $\varepsilon \geq 0.3$), the refinement of the microstructure provides more preferential sites for coarsening and shorter diffusion distances, such that a much coarser cementite distribution is achieved. Unlike in the non-deformed microstructures, where the fragmented cementites preserve their lamellar morphology to a certain extent, in deformed samples the cementites located inside the original pearlite colonies exhibit quite globularized shapes (*i.e.*, low aspect ratios).

The cementite mean aspect ratio variation is shown in Figure 5 as a function of the imposed deformation and annealing treatment time. There are some differences between the coarse and fine initial pearlite conditions. With regard to the coarse pearlite (Figure 5(a)), the mean aspect ratio decreases when the treatment time in the non-deformed condition is prolonged. In contrast, this effect is less perceptible when the treatment is applied to deformed samples. This evolution in mean aspect ratio may indicate that the microstructure is close to reaching the fully fragmented condition with the short annealing cycle. In the non-deformed microstructure, as the break-up occurs more slowly and the microstructure is far from being globularized, the fragmentation progresses continuously as the treatment time is extended. In the case of fine pearlite, the differences are less relevant (Figure 5(b)). There is a small decrease in mean aspect ratio with applied deformation before annealing and the differences between both treatment conditions practically disappear.

The evolution of fragmentation and dissolution of cementite particles as a function of applied strain/annealing conditions has been evaluated by measuring the density of cementite particles with an area smaller than 0.02 μm^2. This value was arbitrarily selected, but it offers a good indication of the solubility in the matrix in each strain and annealing time condition since the smallest cementites are first dissolved into the matrix when annealing. The analysis was carried out for the case of coarse pearlite and the results are indicated in Figure 6. The small particle density remains nearly unchanged in the non-deformed condition during soft annealing treatments. In contrast, in the deformed samples the situation is different. The deformation and consequent lamellar cementite break-up leads to a high small cementite particle density in comparison to that measured in the non-deformed condition. After either a short or long annealing cycle, the fine cementite particle density decreases. On the other hand, the higher the deformation imposed, the lower the small cementite particle density before the annealing treatment. Such differences between $\varepsilon = 0.1$, 0.3, and 0.5 warm deformed microstructures could suggest that cementite dissolution

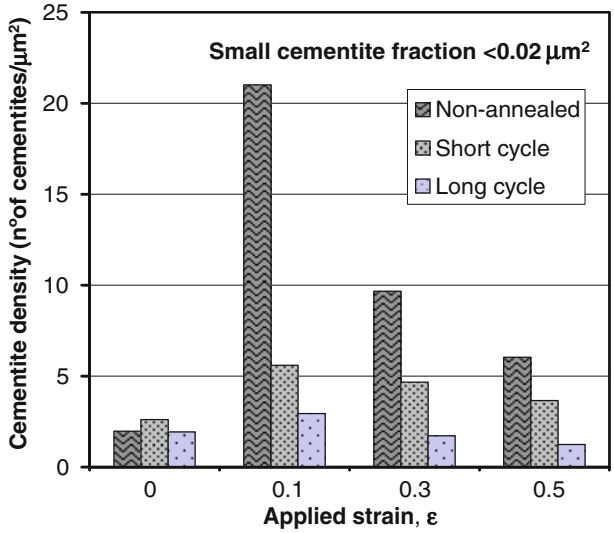

Fig. 6—Fine cementite particle density variation (area <0.02 μm^2) as a function of the applied strain and the duration of the imposed annealing treatment in the case of the initial coarse pearlite microstructure. Short and long cycles correspond to 2 h and 10 h treatments at 993 K (720 °C), respectively.

proceeds dynamically, *i.e.*, while deformation is being applied. Otherwise, if this rapid dissolution of cementite did not occur, a higher particle density would be expected in those cases where a larger deformation was applied. The deformed state of the matrix, together with the relatively high temperatures at which the warm deformation is applied, improves the cementite dissolution in the matrix according to the solute/dislocation interaction in the matrix. Similar behavior has been reported in several studies on pearlitic wire cold drawing, where it was observed that cementite dissolution increased with applied drawing deformation.[25]

The previous analysis can be complemented with the study of the evolution of the particle area fraction distribution with annealing treatment. In Figures 7(a) and (c) the area fraction distributions of cementite particles prior to and after short and long annealing cycles, in both non-deformed and warm deformed conditions ($\varepsilon = 0.3$), are shown for the case of coarse pearlite. The application of the deformation results in a drastic reduction in the fraction of the highest area cementites (compare the distribution corresponding to the non-annealed condition in both figures) and a significant increase in the small-size cementite fractions. Considering the lamellar nature of the coarse pearlite, it may be stated that such diminution in large particles arises from the break-up of the long lamellae during the deformation process.

As Figure 7(a) shows, the static annealing treatment leads to reduction in the high area cementite fractions, and at the same time there is a certain increase in the smaller fractions. This trend is more pronounced the longer the applied treatment is, as can be seen when comparing the distribution after the imposition of the short and long annealing cycles. In the warm deformed case (Figure 7(c)), such a trend is not as evident. The mechanical lamellae break-up during strain application promotes small area cementite formation (see 0 to 0.02 μm^2 fraction). These cementites present high solubility due to their high area to volume ratio, and they dissolve on annealing. The values measured for the cementite fraction constituted by particles with an area larger than 0.10 μm^2 suggest competition between the break-up processes and coarsening phenomena. Break-up processes give rise to the decrease in the largest cementite area fraction after the short cycle. Once the lamellae break-up slows down, the coarsening mechanism gains importance as it is responsible for the increase in the area fraction of large cementites registered after the long annealing cycle.

Figure 7(e) shows the average aspect ratio evolution in each range of cementite sizes, for the non-deformed and warm deformed coarse pearlite cases cited above. The lamellar constitution of the cementites is confirmed by the data, given that the aspect ratio increases at the same time the cementite area does. In the non-annealed condition both show similar average aspect ratio values, but when the annealing cycles are imposed, significant differences may be observed. In either non-deformed or warm deformed coarse pearlites, the average aspect ratio values decrease after the annealing treatments, but in the warm deformed pearlite this reduction is far more significant. While the static annealing cementites still maintain their high aspect ratio lamellar morphology after the long annealing cycle, the warm deformed pearlite shows average aspect ratio values lower than 3 in all the cementite area ranges.

The area fraction distribution for the starting non-deformed fine pearlite microstructure is shown in Figure 7(b). Owing to the shorter length and the lower lamella thickness in comparison with the coarse pearlite (see Table I), the overall cementite area is mainly constituted by relatively small cementites. When the annealing treatment is applied, the cementite fraction constituted by the smallest cementite (0 to 0.02 μm^2 fraction) gradually decreases as treatment time is extended (from short to long cycle), and the area fraction of larger cementite sizes increases. The area fraction distribution after the application of warm deformation ($\varepsilon = 0.3$) is shown in Figure 7(d). The deformation refines the distribution even further, and it mostly consists of cementites in the 0 to 0.02 μm^2 range, the presence of cementites with an area higher than 0.06 μm^2 being scarce. During annealing, the dissolution and coarsening effects reduce the fraction of the smallest cementites and high area of newly created cementites gains importance in the area fraction distribution.

Non-deformed and warm deformed fine pearlite aspect ratio evolution is plotted in Figure 7(f). Similar to the case of coarse pearlite, warm deformation leads to a lower aspect ratio distribution compared to static annealing. When comparing their distribution in the non-annealed condition, it is observed that although the average aspect ratio of the cementites within the 0 to 0.02 μm^2 range is smaller in the warm deformed condition, while unexpectedly the large area cementites exhibit higher aspect ratio values than in the non-deformed microstructure. There is no clear explanation for that, and, therefore, such observation could be ascribable to the lower reliability of the determined value due to the reduced number of cementites in these area ranges (Figure 7(d)).

If the area distributions corresponding to warm deformed coarse and fine pearlite microstructures subjected to long annealing cycle are compared, it could be concluded that the influence of the starting pearlite features loses impact as long as the soft annealing treatment time is extended (see also aspect ratio distributions in Figures 7(e) and (f) after a long annealing treatment).

The degree of spheroidization, measured in terms of spheroidized area fraction, is represented in Figure 8 for both initial pearlite conditions. The benefits provided by the slight warm deformation are clear when comparing the degree of spheroidization attained after different holding times. As the applied deformation increases, a higher degree of spheroidization is reached independently of the initial pearlite characteristics. Both coarse and fine pearlite microstructures show high sensitivity to deformation, as denoted by the considerable increase of the degree of spheroidization observed even at the lowest deformation of $\varepsilon = 0.1$. It is worth emphasizing that the degree of spheroidization measured in both non-deformed and $\varepsilon = 0.1$ deformed microstructures

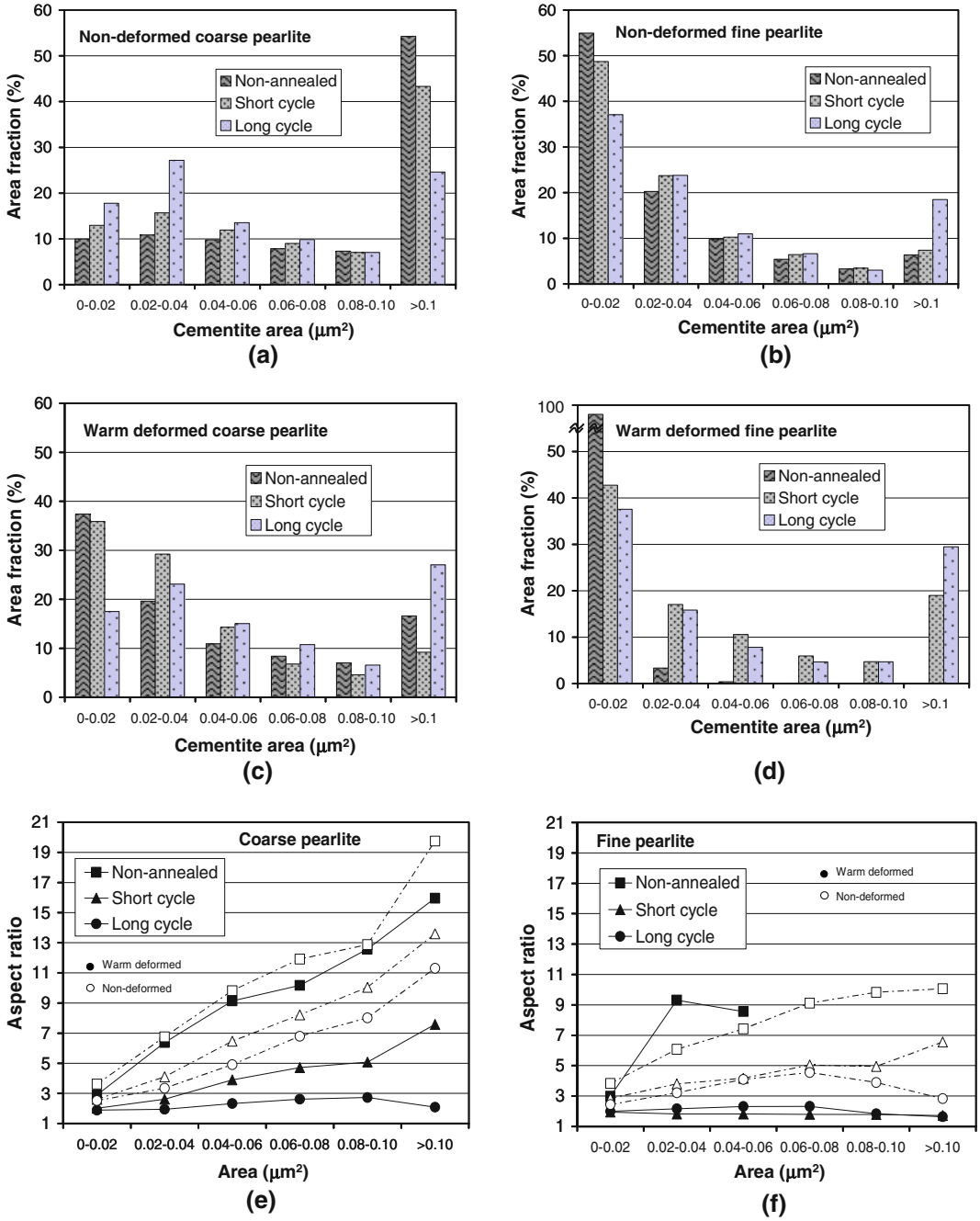

Fig. 7—(*a*, *b*) Cementite size distribution in the non-deformed coarse and fine pearlite, (*c*, *d*) idem in the warm deformed ($\varepsilon = 0.3$) initial coarse and fine pearlite microstructures, and (*e*, *f*) variation of the aspect ratio of the cementites during annealing treatment, in both coarse and fine warm deformed pearlite cases. Values correspond to the non-deformed microstructures (empty symbols). Short and long cycles correspond to a 2-h- and 10-h-long treatments at 993 K (720 °C), respectively.

prior to annealing do not differ significantly. This means that in this case the improvement in the degree of spheroidization associated with warm deformed microstructures after annealing might be mainly attributed to the acceleration of the spheroidization kinetics during heat treatment. It must be also pointed out that at $\varepsilon = 0.1$, the strain is so low that it may not be homogeneously distributed throughout the whole microstructure. Therefore, depending on the pearlite orientation, some colonies may have undergone greater deformation than others, which may result in different behaviors on annealing. At larger deformations of $\varepsilon = 0.3$ and 0.5, mechanical fragmentation is more effective and results in an increase in the degree of spheroidization in the non-annealed condition as well. Mechanical break-up provides very fine cementite particles, characterized by a high surface/volume ratio, a factor that will favor their dissolution in the matrix. It can be also observed that increasing the applied deformation from 0.3 to 0.5 does not lead to very

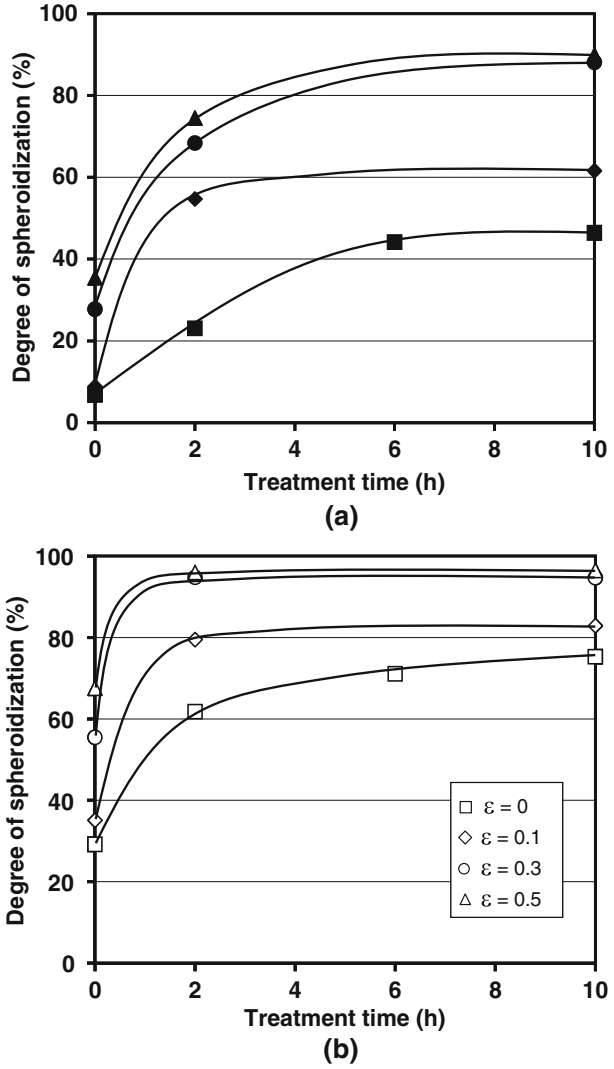

Fig. 8—Evolution of the degree of spheroidization as a function of the holding time at the annealing temperature of 993 K (720 °C) and prior deformation conditioning in (*a*) coarse and (*b*) fine pearlite initial microstructures.

remarkable improvements in terms of the degree of spheroidization.

The initial fine pearlite seems to be more prone to spheroidization than the coarse one, which is in agreement with the expected behavior, given that its lamellae defect density as well as the surface/volume ratio are by far higher. When subjected to the same deformation conditions, the finer pearlite evolves to a more spheroidized microstructure, although the differences become smaller for higher applied deformations and longer annealing time. According to standard ASTM F 2282-03,[26] the initial coarse pearlite microstructure deformed to $\varepsilon = 0.1$ and spheroidized for 10 hours attains a G2 IFI spheroidization rating. Based on that, the obtained microstructure would be suitable for light upsetting processes. When larger deformation is applied an almost fully spheroidized microstructure, G1, is developed after the long annealing cycle, which, according to this criterion, qualifies the microstructure as appropriate for heavy upsetting or extrusion. As for the deformed fine pearlite, spheroidization proceeds so quickly that the G1 degree is reached just after performing the short cycle.

Regarding the deformability of the steel, it has been reported that it depends on the degree of spheroidization and rather than hardness or cementite particle size.[1] Consequently, it could be concluded that the slightly warm deformed and annealed steels could offer better cold forming properties than the steels obtained by the static conventional route.

B. *Cementite Spheroidization Mechanisms*

In conventional soft annealing treatments, it is widely accepted that the morphological changes in the lamellar cementites are related to the presence of crystalline defects in the lamellae.[17,18] Defects such as lamella terminations, kinks, and holes provide high curvature areas from which spheroidization initiates. The lamellae break-up in Figures 3(a) and (b) may arise in part from the existence of such imperfections in the cementite after isothermal phase transformation at 973 K and 903 K (700 °C and 630 °C). Essentially, spheroidization may be considered to rely on the Gibbs-Thompson effect, which is responsible for the continuous solute flux between high curvature areas and flat zones of the lamella. Thus, the continuous migration of the defect would end up causing the observed lamella splitting. The initial lamellae fragmentation involves an increase in the lamella termination density and could give rise to the formation of either globular shapes or shorter but still lamellar forms, in which the process may initiate again. When phase transformation has taken place at temperatures close to the critical temperature A_{c1}, as in the case of coarse pearlite microstructure, the cementites exhibit low defect density. The break-up progresses more slowly than in the finer pearlite, which will present a higher density of defects, and, therefore, long and straight lamellae may remain even after the long annealing cycle (Figure 4(a)). In such a case, together with the fault migration mechanism, the Rayleigh instability phenomenon gains importance in the spheroidization process in the long term, as high aspect ratio cementite plates persist after the initial stages of the annealing treatment.[20,21] This could be the situation that corresponds to the non-deformed coarse pearlite after a short annealing treatment (Figure 5(a)).

The application of warm deformation, in addition to promoting lamellae fragmentation, develops kinks and striations on the lamella that constitute preferential points for further cementite plate splitting (Figure 3). In addition, the dislocation density may increase in both the ferritic matrix and the cementite/ferrite interphase, accelerating the Ostwald ripening phenomenon and leading to a coarser cementite particle distribution during annealing, as confirmed by the results in Figure 7. On the other hand, Rayleigh instability process may be expected to be irrelevant in warm deformed microstructures given that laminar morphology disintegrate quickly, mainly in the cases corresponding to fine pearlite and high applied strain (Figure 7).

Although the cementite defect density increases as the applied strain increases, the migration of defects is not considered to be the predominant break-up mechanism in warm deformation-assisted spheroidization. Instead, it is established that the fragmentation takes place principally according to the thermal groove theory, which provides quick lamella splitting at the annealing temperature.[18,19,22] In order to capture the morphological changes prior to lamellae splitting, warm deformed fine pearlite microstructure was subjected to low-temperature annealing at 873 K (600 °C) for 2 hours. Figure 9 shows a detail of the lamella fracture process in this sample, where partially and fully fragmented cementite lamellae can be observed. The employed temperature is low enough to slow down the advance of spheroidization, such that some cementites on the verge of splitting can be identified (circled area line in the micrograph). This would represent the situation of the fragmented lamella prior to splitting, which is indicated by the straight line in the same micrograph. The micrograph offers a transversal view of the lamella, in which it can be observed that some zones coarsen at the expense of the necking in other zones (see arrows). The observed features in the micrograph would be in good agreement with the expected changes according to the model proposed by Malzahn Kampe *et al.*,[22] and, therefore, it could be stated that the observed necking

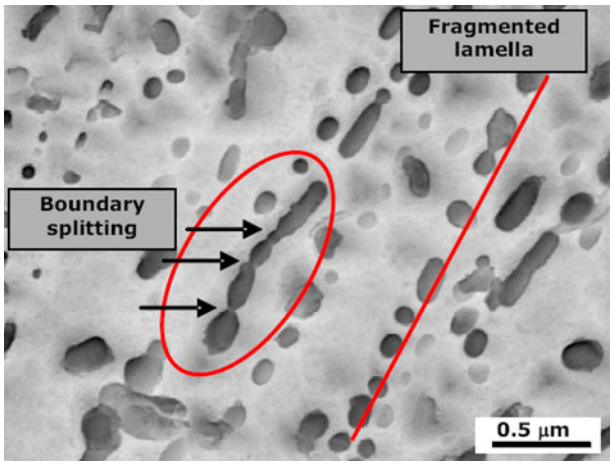

Fig. 9—Detail of the lamella fracture process following the boundary splitting mechanism. Fine pearlite warm deformed ($\varepsilon = 0.3$) and annealed for 2 h at 873 K (600 °C).

effects progress over previously formed channels. In the samples corresponding to non-deformed pearlite microstructures, such prior break-up morphologies have not been observed. Consequently, the strain accumulated by transformation may not be sufficient to develop a substructure in the cementite, especially when phase transformation is conducted under low undercooling conditions.

The whole break-up process related to the observed morphological changes in a warm deformed lamella is schematized in Figure 10. In the first step, the applied deformation promotes the formation of certain substructures inside the lamellae that act as a seed for splitting (Figure 10(a)). The process initiates at triple points between the cementite subgrains and the ferrite matrix, leading to the formation of channels along the sub-boundary (Figure 10(b)). This situation may correspond to the cementite circled in Figure 9. The channels set a continuous solute flux from the triple points to the flat adjacent areas in the lamella, owing to the curvature difference, which finally causes cementite splitting along the channel (Figure 10(c)). After break-up, new cementites are susceptible to undergo edge spheroidization, which would give rise to subsequent fragmentation in even smaller units, or cylinderization, when the aspect ratio of the transversal section is low. Independently of which is the case, the fragmentation results in elongated cementite shapes. These shapes are essentially constituted by cylindrical morphologies, and, therefore, they are unstable against Rayleigh perturbation and split into globular forms (Figure 10(d)).[18–21]

Microstructural analysis shows that edge spheroidization progresses faster in the lamella terminations located at prior austenite grain boundaries, or at boundaries between colonies. Figure 11 illustrates several examples of this coarsening process. In the figure, the A region corresponds to a case of edge spheroidization before lamellae splitting takes place. The B zones correspond to a later stage of the process where it can be observed that once the lamellae have split from the coarsened part located at the boundary, the new terminations undergo edge spheroidization, followed by recession. The lamellae edge splitting mechanism is schematized in Figure 12. The starting situation is shown in Figure 12(a), where the boundary between two pearlite colonies is represented by a dark line. As grain boundaries provide easy paths for pipe diffusion, solute migration proceeds very quickly. Thus the edges

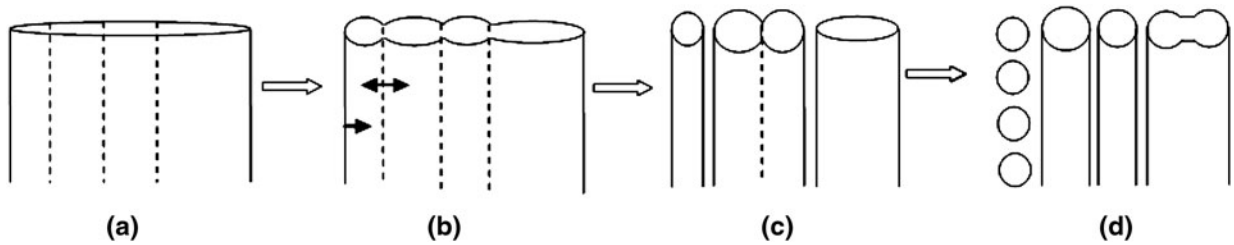

Fig. 10—Scheme of the formation of channels along the lamella and final fragmentation into smaller units: (*a*) sub-boundary development by the applied strain, (*b*) solute diffusion from grooves to flat areas, (*c*) lamella splitting, and (*d*) fragmentation according to Rayleigh instability (adapted from Ref. [22]).

continuously coarsen, forming a ridge along the border of the cementite plate (Figure 12(b)). Spontaneously the flat area splits from the ridge due to the shape instability at the joint and new lamellae edges are formed (Figure 12(c)). The ridges are unstable and decompose in globular cementites according to the Rayleigh perturbation theory illustrated in Figure 10(d), whereas the newly formed edges undergo spheroidization followed by a recession. The globular cementites at the boundaries may either coalescence and coarsen or dissolve during soft annealing, as indicated in Figure 12(d).

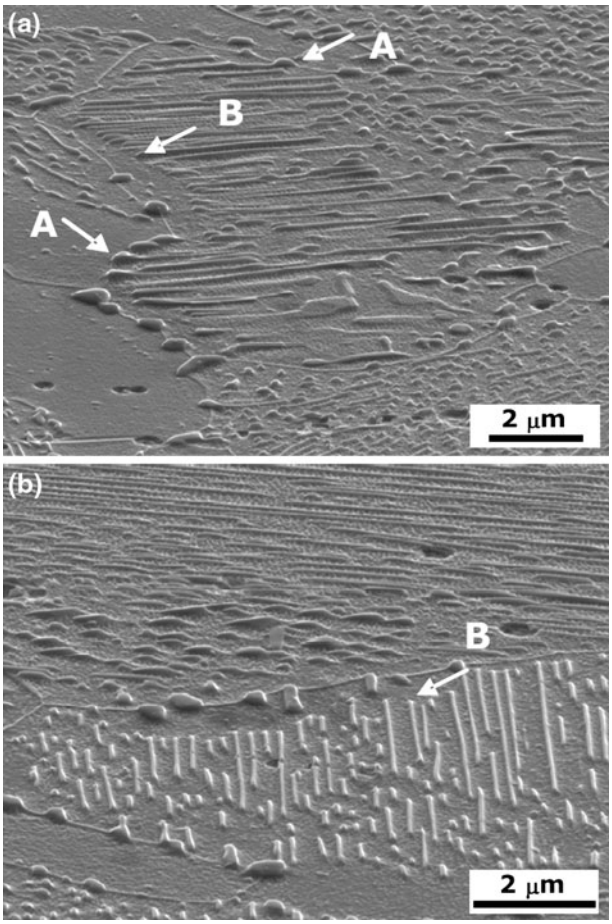

Fig. 11—Detailed micrographs of edge spheroidization due to the quick solute diffusion through the boundary. *A* indicates zones where edge spheroidization before lamellae splitting has taken place and *B* the areas where lamellae recession occurs. Coarse pearlite non-deformed and subjected to a short annealing cycle [2 h/993 K (720 °C)].

It should be noted that the contribution of this process to spheroidization may become more relevant as boundary density increases. This can be the case when smaller austenite grain sizes prior to transformation or enhanced nucleation during phase transformation occur. This effect could explain the improvements in terms of spheroidization associated with pearlitic microstructures formed from fine grained austenite microstructures.[15,27] As we will justify later on, recovery and recrystallization phenomena on warm deformed microstructures will also contribute to increase the boundary density in the matrix (Figure 4).

C. *Microstructure Evolution of the Ferrite Matrix*

In addition to the changes observed in the cementite morphology, the ferrite matrix evolves during annealing treatment, especially in the warm deformed conditions. It is established that in the proeutectoid ferrite, the recovery and subsequent recrystallization proceeds quickly.[11] In the pearlitic matrix, these phenomena take place slowly and gradually as spheroidization progresses, leading to a continuous recrystallization process.[11,13–15] Those areas, where pearlite colonies appear highly decomposed and the cementite density is low, recrystallized first on annealing (see examples in Figures 4(g) and (h)). The continuous nature of the recrystallization may be related to the presence of cementites in the microstructure. Thus, as long as spheroidization and Ostwald ripening processes advance, the pinning effect exerted by the cementites decreases and the subgrain structure formed after recovery may grow.

The image quality maps obtained by the EBSD technique corresponding to the coarse pearlite warm deformed ($\varepsilon = 0.3$) prior to annealing and after long annealing cycle are shown in Figures 13(a) and (c). The low-angle crystallographic misorientation boundaries (between 2 and 15 deg) are highlighted in red and high-angle boundaries (higher than 15 deg) are in black. In the image quality map corresponding to the non-annealed condition (Figure 13(a)), low-angle boundaries appear mainly elongated in a direction close to the perpendicular to the applied stress, and in some cases in

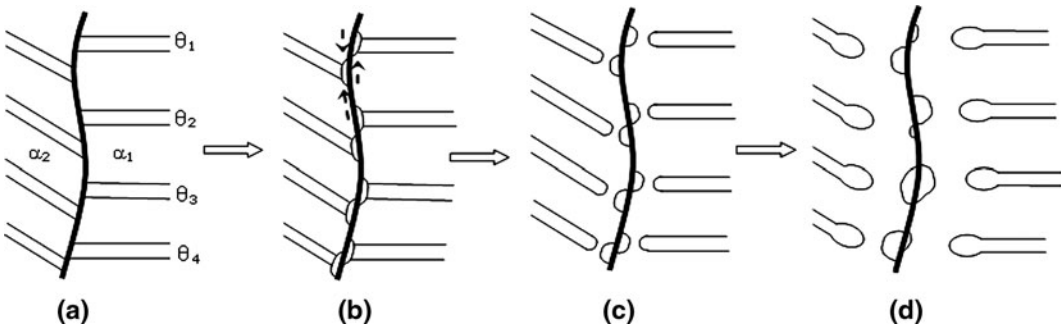

Fig. 12—Scheme of the break-up process according to cementite edge spheroidization along the boundary.

parallel arrangement. These elongated sub-boundaries are located in the interfaces between ferrite and cementite inside certain pearlite colonies, so it may be concluded that lamellar cementite acts as a barrier for dislocation movement during matrix recovery. Nevertheless, due to the high stacking fault energy in the ferrite, recovery and the subsequent subgrain structure development take place easily in the areas where cementite is highly spheroidized.[14] Figure 13(b) shows the existence of the previously mentioned restored areas in the non-annealing condition. As it can be observed, these areas are mainly constituted by globular cells of around 0.5 μm in diameter (center part of the figure).

When the deformed microstructure is subjected to the annealing treatment, cementite spheroidization and dissolution/coarsening allow recovery to occur, and well-defined subgrain microstructure develops in the matrix (Figure 13(c)). Subgrain formation is likely to be a consequence of the combined effects of recovery and cementite lamellae break-up and dissolution, which allow low-angle grain boundaries to migrate. Despite the driving force for recrystallization being provided by the deformation energy, the pinning effect exerted by the cementites reduces low-angle boundary mobility, so that recrystallization occurs in a continuous way as these cementites globularize and coarsen. The micrograph in Figure 13(d) shows the cited restored microstructure in the spheroidized sample and some recrystallized regions are also noticeable in Figures 13(c) and (d).

The inverse pole figure maps of the coarse and fine pearlite microstructures deformed at different levels are shown in Figure 14 for the condition corresponding to 10 hours of annealing treatment. Warm deformation considerably refines the grain size of the spheroidized microstructure, confirming the higher degree of recrystallization occurrence as the applied deformation increases. Greater refinement is observed in the case of fine pearlite, although at none of the considered conditions has recrystallization been completed. Figure 15 shows the average ferrite grain sizes determined by EBSD in each warm deformation condition after the long annealing cycle. The differences in ferrite grain size between fine and coarse pearlite microstructures diminish as the applied warm deformation increases.

A certain loss on the deformability as the ferrite grain size is reduced has been reported, which could arise from the greater difficulty in forming dislocation pile-ups in small grains.[28] However, for the grain size reductions observed in Figure 15 a weak effect on cold formability could be expected.[29]

D. *Hardness Evolution During Spheroidization*

The evolution of hardness as a function of applied strain and annealing conditions is illustrated in Figure 16.

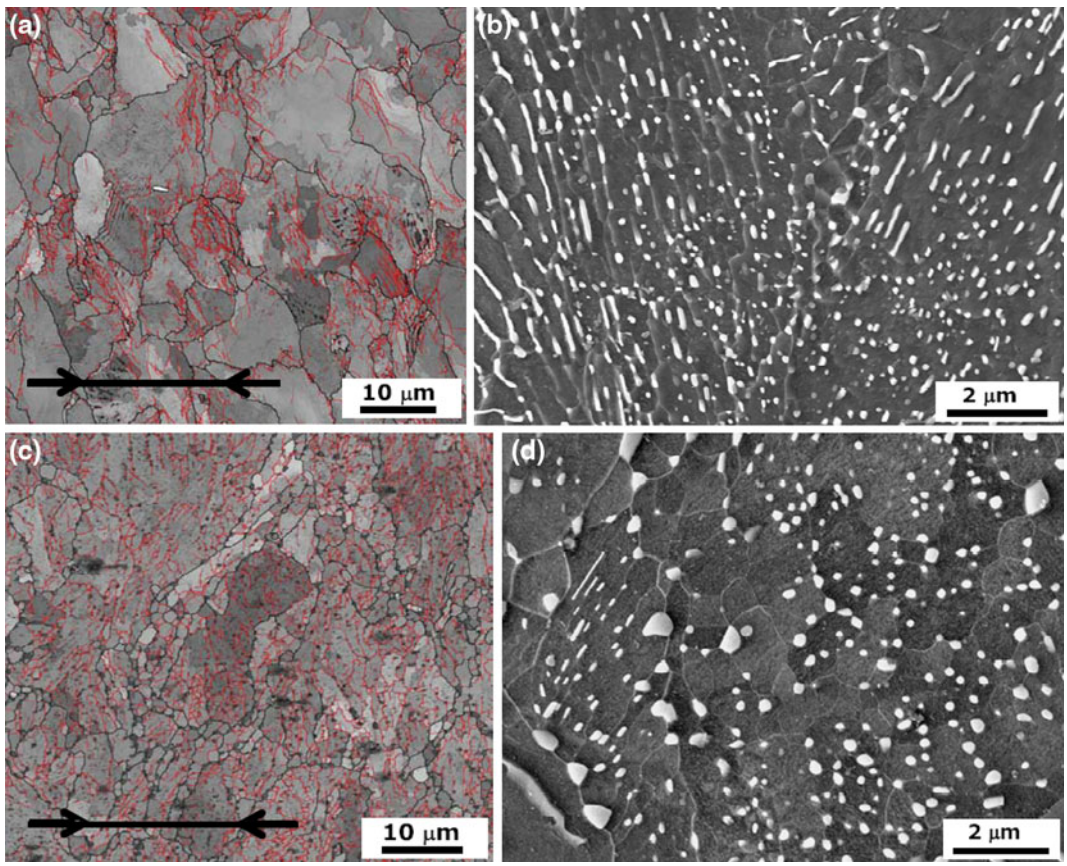

Fig. 13—Image quality maps obtained by the EBSD technique and FEG-SEM micrographs of $\varepsilon = 0.3$ deformed samples (coarse pearlite) in (*a*, *b*) non-annealed and (*c*, *d*) long annealing [10 h/993 K (720 °C)] conditions. Red lines in the image quality maps indicate low-angle grain boundaries (<15 deg), whereas the black lines correspond to high-angle grain boundaries (>15 deg). Arrows indicate the direction of strain application (Color figure online).

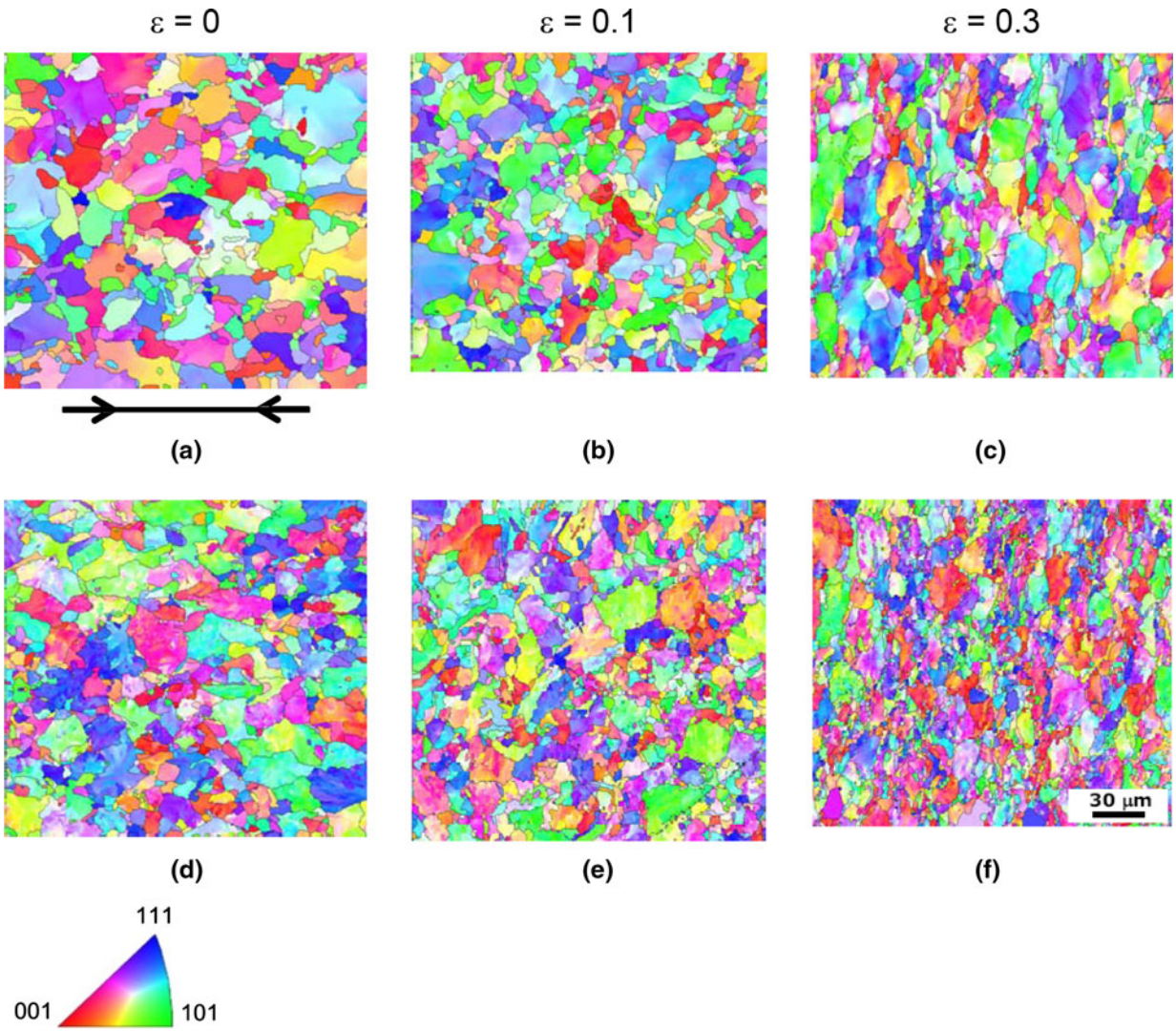

Fig. 14—Image pole figure maps obtained by EBSD technique corresponding to coarse ((*a*) through (*c*)) and fine ((*d*) through (*f*)) pearlite after a long annealing cycle [10 h/993 K (720 °C)]. Arrows in (a) indicate the strain application direction in all the maps.

Both initial pearlite microstructures soften significantly after the annealing treatment, although the main softening occurs after initial holding at the annealing temperature, as evidenced by the small drop in hardness when adopting the long annealing cycle instead of the short one. There are several phenomena that contribute to softening at annealing temperatures.[11,14] The recovery in combination with the cementite lamellae break-up and dissolution are likely to be responsible for the high hardness drop observed in the short term. At a longer maintenance time, the softening is slowed down since the microstructure, in the case of the deformed conditions, is already restored, and the contribution to softening is related to Ostwald ripening and to continuous recrystallization. These processes, despite producing evident microstructural changes, do not contribute very significantly to softening, and, therefore, little drop in hardness may be expected from extending the heat treatment beyond 10 hours.

With regard to the initial pearlite features, it is observed that fine pearlite, in spite of being more prone to spheroidization, exhibits higher hardness values than coarse pearlite, independently of the applied deformation. This difference may be related to the higher strain stored in the fine pearlite because of the lower temperature at which it has been formed and deformed and the lower proeutectoid soft ferrite fraction present (see Table I), which counteracts the overall softening associated with spheroidization. With the exception of the case of non-deformed coarse pearlite, all the different microstructures under study attain quite similar hardness values after long annealing treatment. In spite of the benefits in terms of hardness when extending the treatment time beyond 10 hours, it must be considered that the continuous cementite coarsening could reduce the pinning effect, favoring the occurrence of abnormal grain growth (some isolated coarse grains have been identified after 10 hours of treatment in the initial fine pearlite microstructure). In such a situation, even

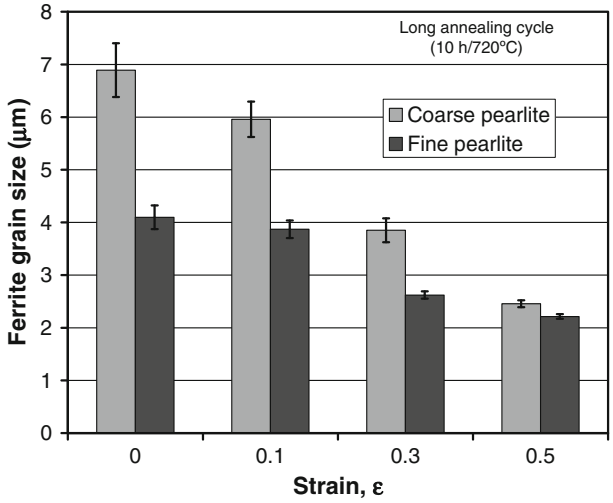

Fig. 15—Average ferrite grain size measured by the EBSD technique in both fine and coarse initial warm deformed microstructures after the application of a long annealing cycle [10 h/993 K (720 °C)].

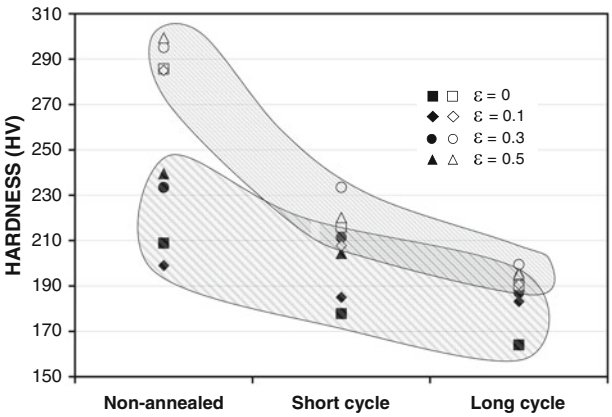

Fig. 16—Hardness values of the different microstructures analyzed after short [2 h/993 K (720 °C)] and long cycle [10 h/993 K (720 °C)] soft annealing treatments for coarse (closed symbols) and fine (open symbols) pearlite.

though additional softening could occur, the resulting microstructure might be detrimental from the perspective of good cold formability. It must be considered that abnormal grains are weak microstructural features since crack propagation along their length is favored.[30] In light of this, the duration of the annealing should be adjusted with the aim of satisfying not only a minimum hardness but also a proper grain microstructure.

IV. CONCLUSIONS

Slight warm deformation promotes faster and enhanced cementite spheroidization, and hence high degrees of spheroidization are obtained after annealing cycles that are shorter than the conventional duration. The higher the warm deformation, the higher the degree of spheroidization after annealing. When warm deformations $\varepsilon \geq 0.3$ are introduced, almost fully spheroidized microstructures with a degree of spheroidization higher than 90 pct may be obtained with either the coarse or fine pearlite initial microstructures. The initial coarse pearlite microstructure requires long annealing cycles to achieve that degree. In this case the application of small strains ($\varepsilon = 0.1$) is not sufficient to provide such a high degree of spheroidization, although a significant improvement is obtained compared to the static annealing (non-deformed) situation. Fine pearlite initial microstructure is easier to spheroidize and a degree of spheroidization of 90 pct can be reached after short annealing cycles for deformations larger than $\varepsilon = 0.3$. For lower strains such a degree of spheroidization cannot be reached even after the longest annealing cycle.

It has been confirmed that the lamellae break-up takes place in warm deformed pearlite spheroidization in accordance with the thermal groove theory. Lamellae edges located at boundaries undergo accelerated coarsening owing to the enhanced pipe diffusion. Continuous coarsening causes a ridge to form, involving consequent morphological instability with respect to the adjacent flat area of the lamella. This instability is followed by splitting and a subsequent recession of the cementite plate, resulting in a coarser cementite distribution.

The initial fine pearlite microstructure induces faster spheroidization in all the conditions, independently of the warm deformation applied. The difference between coarse and fine pearlite microstructures arises from the higher defect density present in the latest.

Warm deformation leads to ferrite grain size refinement after annealing. Grain refinement takes place *via* the continuous recrystallization process, which is controlled by cementite spheroidization and coarsening.

The advantage of the reduction in spheroidization time given by the application of warm deformation is, to some extent, counteracted by an increase in hardness values compared to conventional treatments. Nevertheless, the increase in hardness in comparison with non-deformed conventional samples is not excessive after the long annealing treatment, especially for the starting fine pearlite microstructure where the application of the warm deformation results in hardness increase lower than 5 pct.

The combination of the applied warm deformation and the annealing cycle duration leads to a wide range of steel conditioning prior to cold forming processes. Considering the hardness, degree of spheroidization, and ferrite grain size refinement, the best combination would be the one involving initial fine pearlite with an applied strain of 0.3 or higher and a long annealing treatment [10 hours/993 K (720 °C)]. A similar hardness and degree of spheroidization could be also obtained when considering the initial coarse pearlite microstructure, although a coarser ferrite grain size distribution results.

ACKNOWLEDGMENTS

Partial financial support of this work by the Spanish Science and Innovation Department (CICYT MAT2010-17672 project) is acknowledged.

REFERENCES

1. J.M. O'Brien and W.F. Hosford: *Metall. Mater. Trans. A*, 2002, vol. 33A, pp. 1255–61.
2. E. Karadeniz: *Mater. Des*, 2008, vol. 29, pp. 251–56.
3. S. Chattopadhyay and C.M. Sellars: *Acta Metall.*, 1982, vol. 30, pp. 157–70.
4. D. Hernandez-Silva, R.D. Morales, and J.G. Cabañas-Moreno: *ISIJ Int.*, 1992, vol. 32, pp. 1297–1305.
5. H.L. Yi, Z.Y. Hou, Y.B. Xu, D. Wu, and G.D. Wang: *Scripta Mater.*, 2012, vol. 67, pp. 645–48.
6. Ch. Zheng, L. Li, W. Yang, and Z. Sun: *Mater. Sci. Eng. A*, 2012, vol. A558, pp. 158–61.
7. A. Saha, D.K. Mondal, K. Biswas, and J. Maity: *Mater. Sci. Eng. A*, 2012, vol. A541, pp. 204–15.
8. N.V. Luzginova, L. Zhao, and J. Sietsma: *Metall. Mater. Trans. A*, 2008, vol. 39A, pp. 513–21.
9. G. Krauss: *Steel: Processing, Structure and Performance*, ASM International, Materials Park, OH, 2005.
10. J.P. Ferrer, C. Capdevila, F.G. Caballero, and C. Garcia de Andres: *International Conference on Advances in Materials and Materials Processing*, 2006, pp. 500–06.
11. R. Song, D. Ponge, D. Raabe, J.G. Speer, and D.K. Matlock: *Mater. Sci. Eng. A*, 2006, vol. A441, pp. 1–17.
12. L. Storojeva, R. Kaspar, and D. Ponge: *ISIJ Int.*, 2004, vol. 44, pp. 1211–16.
13. N. Tsuji and T. Maki: *Scripta Mater.*, 2009, vol. 60, pp. 1044–49.
14. K. Handa, Y. Kimura, Y. Yasumoto, T. Kamioka, and Y. Mishima: *Mater. Sci. Eng. A*, 2010, vol. A527, pp. 1926–32.
15. L. Storojeva, D. Ponge, R. Kaspar, and D. Raabe: *Acta Mater.*, 2004, vol. 52, pp. 2209–20.
16. J. Arruabarrena, P. Uranga, B. López, and J.M. Rodriguez-Ibabe: *MS&T '11 Conference Proceedings*, 2011, pp. 698–705.
17. Y.T. Wang, Y. Adachi, K. Nakajima, and Y. Sugimoto: *Acta Mater.*, 2010, vol. 58, pp. 4849–58.
18. Y.L. Tian and R.W. Kraft: *Metall. Trans.*, 1987, vol. 8A, pp. 1403–14.
19. G. Sharma, R.V. Ramanujan, and G.P. Tiwari: *Acta Mater.*, 2000, vol. 48, pp. 875–89.
20. E. Werner: *Acta Metall.*, 1989, vol. 37, pp. 2047–53.
21. S. Chattopadhyay and C.M. Sellars: *Metallography*, 1977, vol. 10, pp. 89–105.
22. J.C. Malzahn Kampe, T.H. Courtney, and Y. Leng: *Acta Met.*, 1989, vol. 37, pp. 1735–45.
23. N. Isasti, D. Jorge-Badiola, M.L. Taheri, B. Lopez, and P. Uranga: *Metall. Mater. Trans. A*, 2011, vol. 42A, pp. 3729–42.
24. W.J. Nam and C.M. Bae: *Scripta Mater.*, 1999, vol. 41, pp. 313–18.
25. V.G. Gavriljuk: *Mater. Sci. Eng. A*, 2003, vol. A345, pp. 81–89.
26. ASTM F2282-03: Standard Specification for Quality Assurance Requirements for Carbon and Alloy Steel Wire, Rods, and Bars for Mechanical Fasteners, ASTM International.
27. K. Aihara and S. Kanbara: *The Sumitomo Search*, 1990, vol. 42, pp. 1–8.
28. M. Calcagnotto, D. Ponge, Y. Adachi, and D. Raabe: *Acta Mater.*, 2011, vol. 59, pp. 658–70.
29. ICFG document No 11/01: *Steels for Cold Forging-Their Behavior and Selection*, Meisenbach Verlag, ISBN 3-87525-148-2, Bamberg, 2001.
30. J.M. Rodriguez-Ibabe: *Mater. Sci. Forum*, 1998, vols. 284–286, pp. 51–62.